Research Article | Vol. 28, No. 13 / 22 June 2020 / Optics Express 19074

Optics EXPRESS

Light-induced thermo-elastic effect in quartz tuning forks exploited as a photodetector in gas absorption spectroscopy

STEFANO DELLO RUSSO,[1,2] ANDREA ZIFARELLI,[1,2] PIETRO PATIMISCO,[1,2] ANGELO SAMPAOLO,[1,2] TINGTING WEI,[1] HONGPENG WU,[1] LEI DONG,[1,3] AND VINCENZO SPAGNOLO[1,2,4]

[1]*State Key Laboratory of Quantum Optics and Quantum Optics Devices, Institute of Laser Spectroscopy, Shanxi University, Taiyuan 030006, China*
[2]*PolySenSe Lab- Physics Department, Università degli Studi di Bari and Politecnico di Bari, CNR-IFN, Via Amendola 173, Bari 70126, Italy*
[3]*donglei@sxu.edu.cn*
[4]*vincenzoluigi.spagnolo@poliba.it*

Abstract: We report on a study of light-induced thermo-elastic effects occurring in quartz tuning forks (QTFs) when exploited as near-infrared light detectors in a tunable diode laser absorption spectroscopy sensor setup. Our analysis showed that when the residual laser beam transmitted by the absorption cell is focused on the QTF surface area where the maximum strain field occurs, the QTF signal-to-noise ratio (SNR) is proportional to the strain itself and to the QTF accumulation time. The SNR was also evaluated when the pressure surrounding the QTF was lowered from 700 Torr to 5 Torr, resulting in an enhancement factor of ∽4 at the lowest pressure. At 5 torr, the QTF employed as light detector showed an SNR ∽6.5 times higher than that obtained by using a commercially available amplified photodetector.

1. Introduction

Tunable diode laser absorption spectroscopy (TDLAS) has served as useful tool for molecular spectroscopy, capable of achieving quantitative and selective spectroscopic measurements of a large number of gas species. Gas sensors based on TDLAS have been widely used in several applications, including environmental monitoring [1], industrial process control [2,3] and biomedical applications [4]. Gas concentration is retrieved by means of the Lambert-Beer law, in which the measurement of fractional transmission of light (given by the ratio between transmitted and incident light intensity on a gas sample) is related to the target gas concentration and the optical pathlength. Direct detection and wavelength modulation spectroscopy (WMS) are the most common sensing methods of TDLAS. In WMS, the current modulation of the laser radiation produces both a frequency and an intensity modulation of the radiation transmitted through the cell. Then, the spectral component of the photodetector signal at the modulation frequency (or higher harmonics) is extracted. Thus, only the noise centred at the detection frequency and within the detection bandwidth of the photodetector will affect the measurements. With respect to direct absorption, WMS reduces the noise-equivalent absorbance and in turn improves the minimum detection limit [5], making the WMS final performance strongly dependent on the photodetector properties. Infrared photodetectors can be divided in two main groups: i) thermal detectors (bolometers, pyroelectrics and Golay Cells) in which the absorbed radiation causes a change of a physical property of the sensing material to generate an electrical signal; ii) photonic detectors (photoconductive, photovoltaic and photoemissive) in which the radiation is absorbed by the material via interaction with electrons and an electrical signal results from changes in the electronic distribution [6–8]. Recently, quartz tuning forks (QTFs) have been proposed as

#393292 https://doi.org/10.1364/OE.393292
Journal © 2020 Received 19 Mar 2020; revised 14 May 2020; accepted 25 May 2020; published 12 Jun 2020

Optics EXPRESS

a sensitive and low-cost alternative to infrared optical detectors, exploiting the piezoelectric properties of quartz crystals. Due to the advantage of a high-quality factor Q >10,000 at atmospheric pressure, the detection bandwidth (few Hertz or even lower) is several orders of magnitude narrower than optical infrared detectors [7]. For optical sensing applications, electric charges generation due to laser-QTF interaction was demonstrated exploiting both mechanical momentum transfer and thermo-elastic conversion. In the former case, when the electromagnetic radiation irradiates a QTF prong close to the free end, a transfer of mechanical momentum from the incident photons to the material occurs, i.e. radiation pressure. The deflection of the prong due to energy transfer from the radiation to the mechanical oscillator is enhanced when the incident light is modulated at the resonance frequency of the QTF. This results in a periodic force driving the QTF prong into oscillation [9,10]. This effect is strongly affected by the spot position on the QTF prong, since is crucial to hit an anti-nodal point to enhance the prong deflection. Moreover, laser spot size should be comparable to quartz crystal thickness, typically $\sim 300\,\mu m$. On the other hand, the second method recently proposed by He et al. [11] and Ma et al. [12], exploits light-induced thermo-elastic effect occurring in a QTF as basic physical principle to enable light detection. When the radiation hits the surface of the QTF, photothermal energy is generated because of light absorption by the quartz. Due to the thermo-elastic conversion, elastic deformations put prongs into vibration if the laser is intensity-modulated at one the QTF resonance frequencies [13,14]. This effect is enhanced when the radiation is focused close to the prong clamped end, named hereafter prong base, where the stress field is supposed to be mainly located at [15].

Y. Ma et al. realized a gas sensor based on WMS and light-induced thermo-elastic spectroscopy (LITES) by using a standard 32.7 kHz QTF, reaching a normalized noise equivalent absorption (NNEA) of $7.63{\cdot}10^{-9}$ $cm^{-1}W/\sqrt{Hz}$ [12]. With the same experimental conditions, the NNEA was reduced by one order of magnitude ($9.16{\cdot}10^{-10}$ $cm^{-1}W/\sqrt{Hz}$) by using a custom T-shaped QTF with a resonance frequency of 9.35 kHz [14]. Although an improvement has been reported by employing a custom QTF, literature still lacks a detailed investigation of the dependence of signal-to-noise ratio (SNR) on the geometrical and resonance properties of the QTF and some guidelines to determine theoretically and experimentally the best operating conditions, i.e. laser focus position on the resonator surface, QTF spatial orientation and operating pressure.

In this work, we report a detailed study of the LITES performance with respect to the resonance properties of the QTF. The strain field in the quartz crystal when prongs are forced to vibrate at one of resonance modes was simulated by using COMSOL Multiphysics software with finite element method. A spatial mapping of LITES signal at different laser spot positions experimentally confirms that the higher the strain field, the higher the LITES signal. The dependence of the SNR on the QTF accumulation time was also investigated in all the pressure range from 760 to 5 Torr. Finally, a comparison between the most performing QTF and a commercial InGaAs amplified photodetectors is reported.

2. Experimental setup

The experimental setup for LITES investigation is sketched in Fig. 1. A single-mode continuous-wave pigtailed near-IR laser diode (LD) was used as excitation source. The LD was tuned in order to target a water vapor absorption line falling at $7310.68\,cm^{-1}$ ($1.367\,\mu m$), with linestrength of $8.84{\cdot}10^{-21}$ cm/molecule [16]. The laser beam was coupled with a fiber collimator (OZ Optics LPC-07-1550-9/125-S-0.22-1.01GR-25-3A-1-1) and aligned through a 50 cm-long absorption cell filled with ambient air containing 1% of water vapor. The light transmitted by the cell was focused on the QTF with a lens having a focal length of 50 mm. The laser optical power measured in the focal plane of the lens was 3.5 mW.

A stainless-steel housing equipped with two near-IR windows was realized in order to accommodate and easily replace the QTFs. The housing was fixed to an XYZ translation stage,

Optics EXPRESS

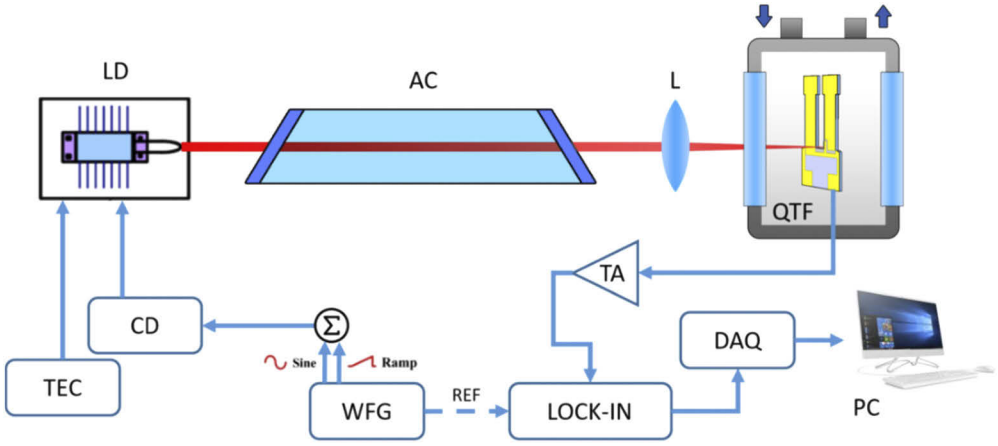

Fig. 1. Experimental setup for optothermal measurements with custom quartz tuning forks (QTFs). LD: Laser Diode, TEC: Temperature controller, CD: Current driver, WFG: Waveform generator, AC: Absorption Cell, TA: Trans-impedance preamplifier, L: focusing Lens, DAQ: Data acquisition card, REF: reference signal, Σ: Adder, PC: Personal Computer.

equipped also with 2-angular degrees of freedom, which allows fine tilt/adjustments of the QTF position with respect to the focused laser beam, whose size was estimated to be ~100 µm. The laser current was modulated at half of the QTF resonance frequency while the QTF signal demodulated at the QTF resonance frequency (WMS and 2f detection). WMS was applied by adding a sinusoidal dither to the laser current driver. A ramp is also applied to the current driver in order to linearly scan the laser wavelength across the water absorption line. In this way, the LITES scan resembles a background-free second derivative of the Lorentzian absorption line. The QTF signal is collected by means of a current-to-voltage converter operational amplifier with feedback resistor $R_f = 10\text{M}\Omega$ and then sent to a lock-in amplifier to be demodulated. The lock-in integration time was set to 100 ms. The demodulated LITES signals were acquired by using a DAQ with an acquisition time set to 300 ms. A vacuum pump and a flow-rate controller (not shown in Fig. 1) were connected to the housing in order to vary and fix the internal pressure from 5 Torr to 700 Torr while maintaining a constant flow in the gas line.

3. Results

As first step, a mapping of the LITES signal at different laser spot positions on the QTF plane was performed. The QTF is positioned on the plane perpendicular to the laser beam direction. The investigated QTF (named hereafter as QTF#1) has a prong length of $L = 10$ mm and width of 0.9 mm, with a crystal thickness of $T = 0.25$ mm. The fundamental mode resonance frequency is 7230.3 Hz, with a quality factor of ~8800 at atmospheric pressure (see Fig. 2(a)), measured by providing a sinusoidal voltage excitation to the QTF, while the laser is off [17–20]. A vibrating prong undergoes several energy dissipations processes due to surrounding medium losses and support losses [21]. When the laser light hits the QTF, close to the base of the prong, additional energy losses affecting the prong vibration can arise from thermo-elastic damping. To evaluate the influence of this damping effect on QTF resonance properties, the frequency and the quality factor were measured via optical excitation (see Fig. 2(b)): the laser was locked to the water absorption peak while the frequency of the current dither was linearly spanned in order to acquire the QTF resonance curve [17]. In this case, the QTF signal is demodulated in 2f mode. The resonance curves obtained with the two methodologies are shown in Fig. 2.

Optics EXPRESS

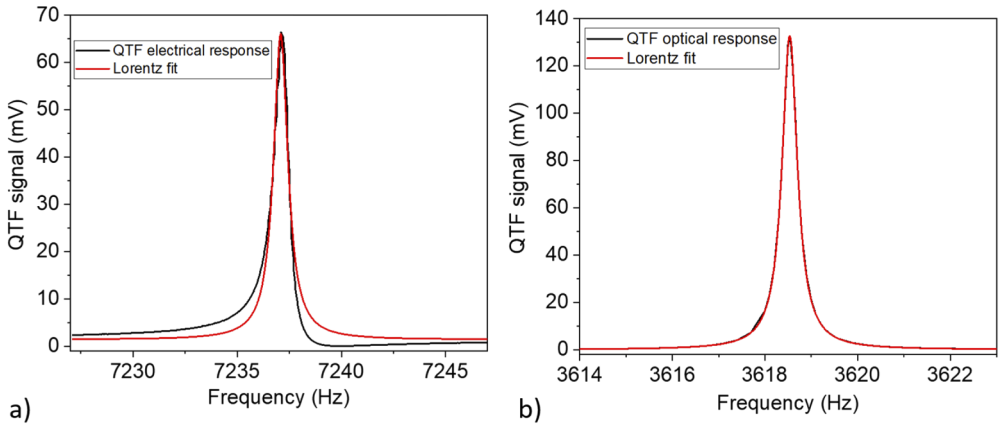

Fig. 2. (a) Electrical and (b) optical characterization performed with QTF#1 operating at the fundamental mode.

The small left-right asymmetry of resonance curve in Fig. 2(a)) is due to parasitic current caused by stray capacitance between the two pins of the QTF when electrically excited. Since this asymmetry arises far from the resonance peak, it does not affect the estimation of QTF resonance properties. The quality factor measured with optical excitation is ~9000, indicating that the electro-mechanical properties of QTF are not affected when the laser radiation impacts on quartz crystal. The QTF first overtone mode was also analysed and showed a resonance frequency of 44,130.8 Hz with a quality factor of ~18,380 at atmospheric pressure.

A 2D map of the LITES signal values at different positions of the laser spot on the QTF plane was then obtained. While the laser beam position is fixed, the QTF is translated along x and y axes on the QTF plane, with a step resolution of 0.5 mm along the x-axis and 0.1 mm along the y-axis. The WMS scheme is adopted with the laser wavelength resonant with the water absorption peak, where the maximum LITES signal occurs.

The map of the LITES signal is reported in Fig. 3, for the QTF vibrating at the fundamental mode (Fig. 3(a)) and at the first overtone mode (Fig. 3(c)). The piezoelectric charges generated by prongs vibrations accumulate where the induced strain is maximum. To calculate the strain spatial distribution when the QTF is forced to vibrate at one of its eigenfrequencies modes, a finite element method (FEM) modelling was implemented using COMSOL Multiphysics. The strain distribution in the QTF plane at the fundamental and overtone mode are shown in arbitrary units respectively in Fig. 3(b) and Fig. 3(d).

From Fig. 3 it can be noted how the map of LITES signal peak values retraces the spatial distribution of the strain field: the maximum LITES signal occurs where the strain reaches its highest values. This correlation is also evident when the QTF vibrates at the first resonance overtone: along the prong edge, the lowest LITES signal occurs at nodes point of the strain field (~2 mm far from the prong base), for both QTF prongs. The same investigation was then performed by replacing QTF#1 with a T-shaped QTF (named hereafter as QTF#2). The T-shaped QTF has 50 µm-deep rectangular grooves carved on both prong sides [22,23] and its geometry is schematized in Fig. 4. The prong has a full length of $L = L1 + L2 = 9.4$ mm, a crystal thickness of $T = 250$ µm, and $W1$ and $W2$ are 2 mm and 1.4 mm, respectively. The fundamental mode has a resonance frequency of 9783.8 Hz and a quality factor at atmospheric pressure of ~11,500.

The map of the LITES signal values and the simulated strain distribution are shown in Fig. 4(a) and 4(b), respectively. As for QTF#1, the spatial distribution of LITES signal shows a good match with the pattern of strain distribution. However, in this case, the highest LITES signal was recorded on the right side of the left prong base (point A in the QTF schematic of Fig. 4). At the

Optics EXPRESS

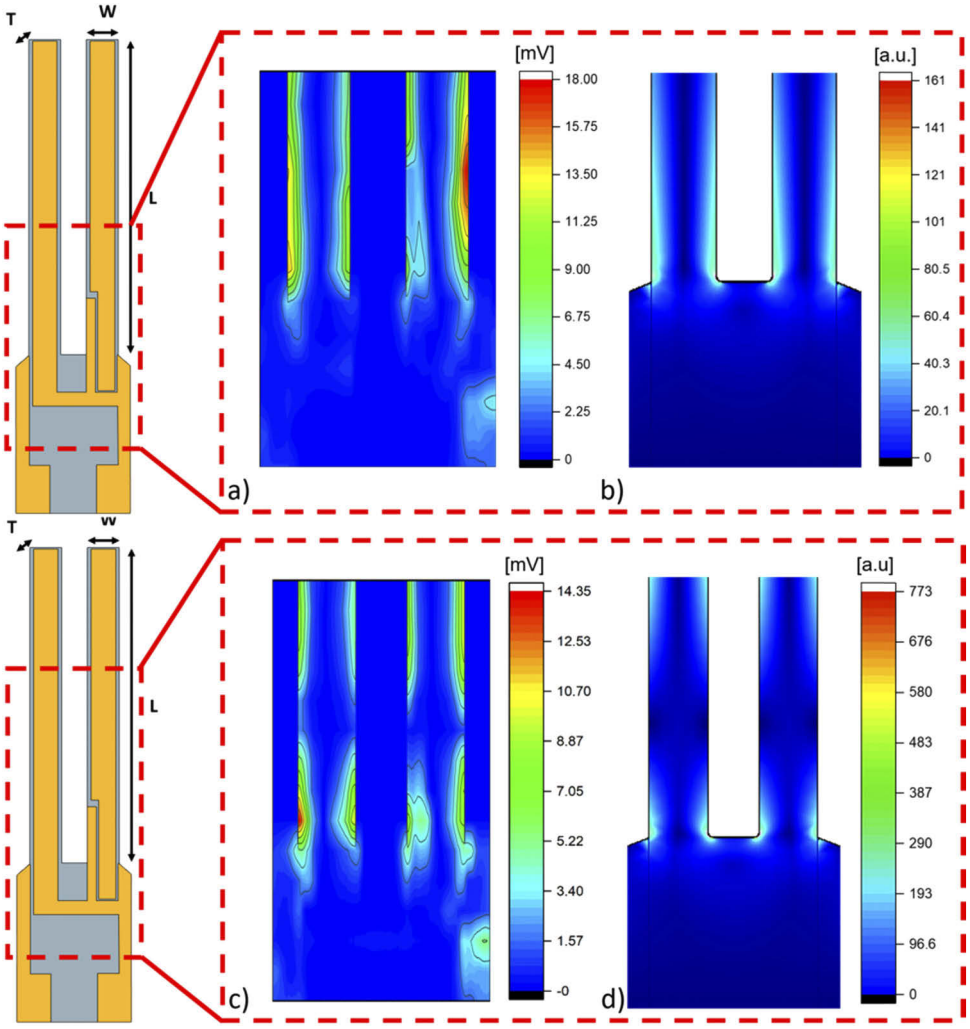

Fig. 3. (a) LITES peak signal mapping and (b) COMSOL simulation of the strain field for QTF#1 fundamental resonance mode. (c) LITES peak signal mapping and (d) COMSOL simulation of the strain field for QTF#1 first resonance overtone mode. LITES signal colour scale reports signal intensities in mV while the intensity of the strain field is reported in arbitrary unit. The LITES signal was mapped only on the QTF surface and not outside of it in order to provide a direct comparison with the simulated strain field.

Optics EXPRESS

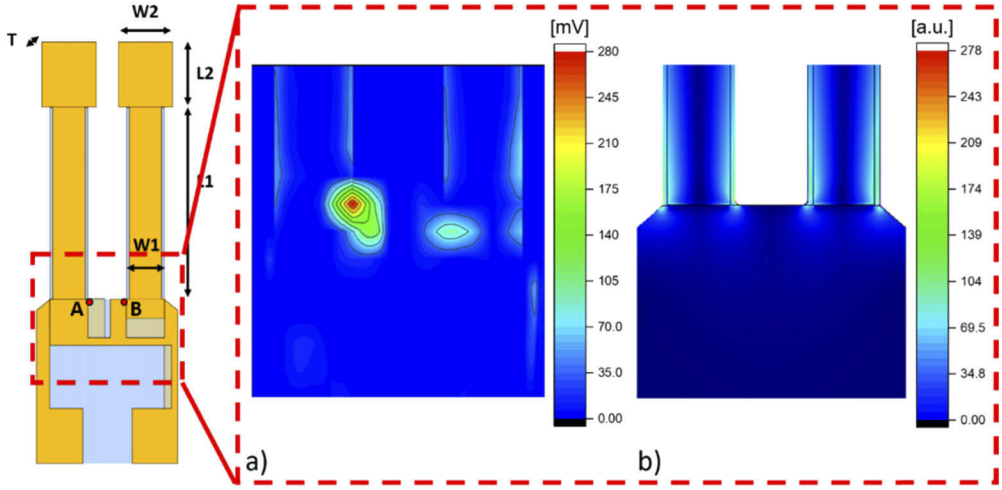

Fig. 4. (a) LITES peak signal mapping and (b) COMSOL simulation of the strain field for QTF#2 fundamental resonance mode. LITES signal colour scale reports signal intensities in mV while the intensity of the strain field is reported in arbitrary unit. The points A and B on the QTF schematic in the left side of the figure indicate the positions of the main local maxima of the LITES signal.

specular point B on the left side of the right prong end the LITES signal is ~4.2 times lower with respect to A. This asymmetry can be ascribed to the gold electrode pattern deposited on the junction area between two prongs. Close to point A, the front surface of this area is uncoated allowing the laser transmission and absorption through the quartz, while on the back side of the QTF a gold film allows the laser beam to be back reflected and diffused. Conversely, close to point B, the gold film on the front surface reflects part of the laser beam, limiting its propagation through the quartz crystal and negatively affecting the LITES signal.

The investigation of the LITES signal on the QTF plane demonstrated its dependence on the strain induced by the prong vibration as well as the influence of the gold layer pattern deposited on the quartz crystal. However, the areas where the maximum strain occurs are not on the QTF plane. These areas are located at the internal side junction of each prong, as shown in the simulation results reported in Figs. 5(a) and 5(b) for QTF#1 and QTF#2, respectively.

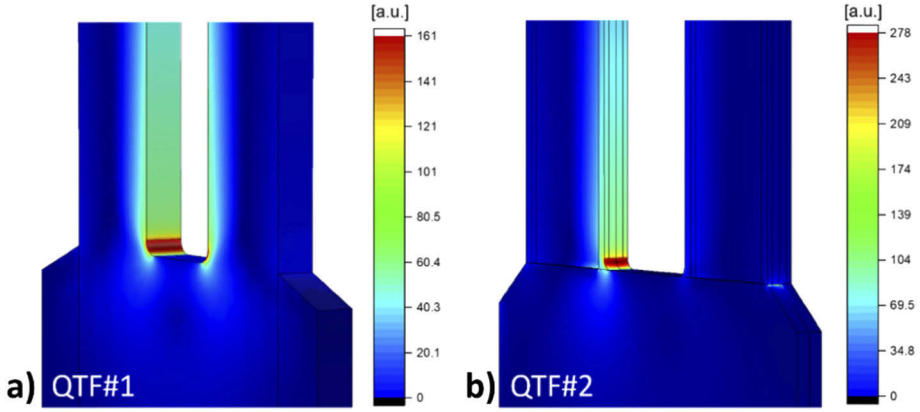

Fig. 5. Zoom and tilt of the COMSOL simulation results in the part of QTF#1 and QTF#2, where the strain has a maximum.

Optics EXPRESS

In order to focus the laser beam upon these areas, the QTF must be rotated along directions identified by an azimuth (φ) and polar (Θ) angle (see Figs. 6(a) and (b)) while the laser beam direction is constantly aligned along the z direction. An extensive investigation of the LITES signals has been performed as a function of both azimuth and polar angles by shining the area located on the internal side of a prong. The LITES signal as a function of the polar angle is reported in Figs. 6(c) and (d).

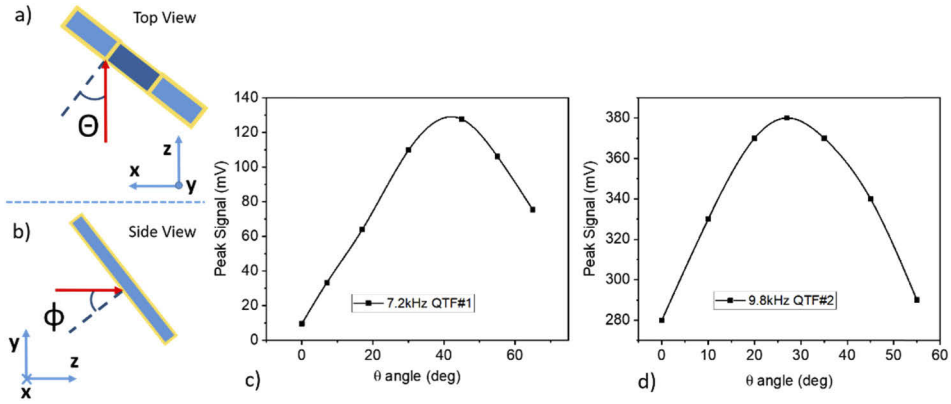

Fig. 6. (a,b) Schematic of the QTFs alignment with respect to the laser beam (red arrow). (c,d) QTF peak signal measured for QTF#1 and QTF#2 respectively, by varying the incidence polar angle. The polar (Θ) and the azimuth (φ) angles measure the rotation of the QTF around the y and the x axes in the zx and zy plane, respectively. Both Θ and φ are measured as the angular separation between the z axis, i.e. the direction of laser propagation, and axis orthogonal to the QTF plane (dashed line). When both φ and Θ are zero, the QTF lies in xy plane while the laser beam is aligned along the z-axis.

As the polar angle increases, the LITES signal rises, reaches a maximum ($\Theta = 45°$ for QTF#1 and $\Theta = 27°$ for QTF#2) and then decreases for larger angles. With respect to in-plane measurement ($\Theta = 0°$) for QTF#1 the LITES signal is enhanced by a factor of ~6.3 when the optimal polar angle is selected, reaching a peak signal of ~127.7 mV. The noise estimation for each QTF was carried out on the peak of the second derivative of the Lorentzian lineshape, by removing the triangular ramp and locking on the absorption peak. Considering a 1σ-noise level of ~0.06 mV, the resulting SNR was ~ 2100. For QTF#2, an enhancement factor of ~1.3 led to a LITES peak signal of ~380.1 mV and a 1σ-noise level of ~0.11 mV, resulting in SNR of ~3380. No significant increases in SNR were recorded when the azimuth angle φ was varied.

The LITES signal is generated by photothermal energy deposited in the quartz crystal because of the light absorption. This energy is then converted in mechanical energy as vibration of prongs at their natural frequencies, i.e. mechanical oscillation. This suggests that the LITES signal should be related to the oscillator accumulation time, defined as the ratio between the quality factor and the angular frequency [20]:

$$\tau = \frac{Q}{2\pi f} \tag{1}$$

For a deeper understanding of the LITES phenomenon, four more custom QTFs were analysed. QTF#3 is a T-shaped QTF with $L = L1 + L2 = 9.4$ mm, $T = 250$ μm, $W1 = 2$ mm and $W2 = 1.4$ mm (see Fig. 4), without grooves [24]. QTF#4 and QTF#5 have rectangular prongs with $L = 1.2$ mm and 1.0 mm, $W = 16.0$ mm and 17.0 mm, respectively, both with $T = 250$ μm. Standard 32.7 kHz-QTF with $L = 3.3$ mm, $W = 330$ μm and $T = 350$ μm was also included. For each QTF, the measured resonance frequency of the fundamental mode and the related quality factor, the

Optics EXPRESS

accumulation time calculated by using Eq. (1) and the maximum strain field ε calculated by using the COMSOL simulation model are reported in Table 1.

Table 1. Electro-mechanical performances and LITES SNR measured for all the QTFs analysed.

QTF	*f [Hz]*	*Q-factor*	*τ [s]*	*ε [a.u]*
QTF# 1	7230.3	8720	0.19	161
QTF# 2	9783.8	11510	0.19	278
QTF# 3	12460.7	10400	0.13	290
QTF# 4	3853.8	7240	0.30	83
QTF# 5	2887.5	5730	0.32	59
STANDARD	32757.4	8630	0.04	532

Then, all QTFs were tested in the LITES setup sketched in Fig. 1. Following the simulation of the strain field, the optimum position of the laser beam in the QTF plane and the polar angle providing the maximum LITES signal were identified. In Fig. 7, the achieved LITES SNRs are plotted as a function of the product between the maximum strain and the QTF accumulation time (see Table 1).

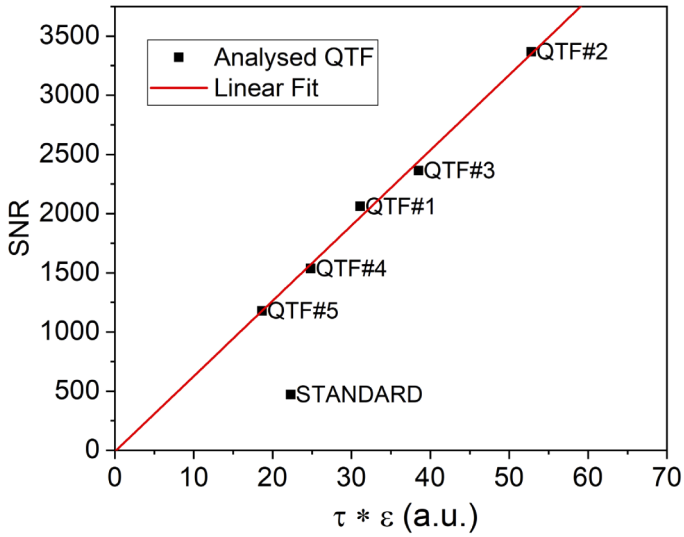

Fig. 7. (Black squares) Calculated SNR as a function the product between accumulation time and strain for all the QTFs analysed. The red line represents the best linear fit.

Apart from standard QTF, LITES SNR values follow a linear trend as a function of the product $\tau \cdot \varepsilon$. The reason of the discrepancy observed for the standard QTF is ascribed to the geometrical dimensions of the standard QTF, which is significantly smaller than the other custom QTFs. Indeed, due to the reduced size of the QTF prongs (330 µm), comparable to laser beam spot size (~100 µm), a precise mapping of the prongs surface area was not possible. As a result, 1σ-noise level measured for the standard QTF was ~0.3 mV, up to 3 times larger than values recorded for the other custom QTFs.

The QTF#2 is the one showing the highest SNR and has been selected for a performance comparison with a commercial photodetector. In the LITES setup (see Fig. 1), with the same experimental conditions, QTF#2 has been replaced by a photodetector (THORLABS PDA10CF-EC) operating in the near-IR [25]. The spectral scans of the water absorption line signals recorded

Optics EXPRESS

with LITES using QTF#2 and acquired with the photodetector are shown in Fig. 8. For an easy comparison, peak values are normalized to the unit for both acquisitions.

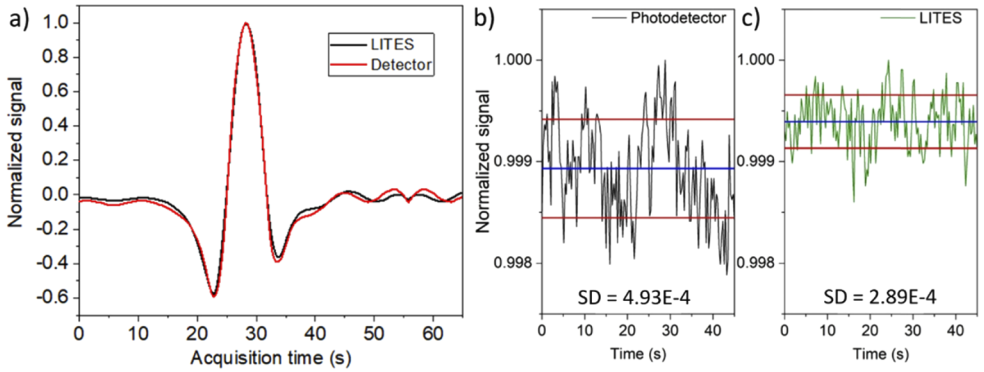

Fig. 8. a) Comparison between normalized QTF#2 LITES signal (black curve) and photodetector signal (red curve). (b) LITES and (c) photodetector signal as a function of time when the laser is locked on the water absorption line. The noise level is extracted as the standard deviation (1σ-value) of the dataset. Being both signals normalized to the unit, the ratio between 1σ-noise levels provides the SNR enhancement of the QTF with respect to the photodetector.

The photodetector peak signal was ~608.25 mV with a 1σ-noise level of 0.3 mV, resulting in an SNR ∽2030, 1.65 times lower than that obtained with QTF#2 (SNR of ~3500, see Fig. 7). This indicates that the QTF can provide higher performance for light detection with respect to commercial amplified photodetectors.

Exploiting the dependence of the LITES SNR from the QTF accumulation time, if lowering the pressure within the QTF housing, an increase of the QTF quality factor is predicted [17] and

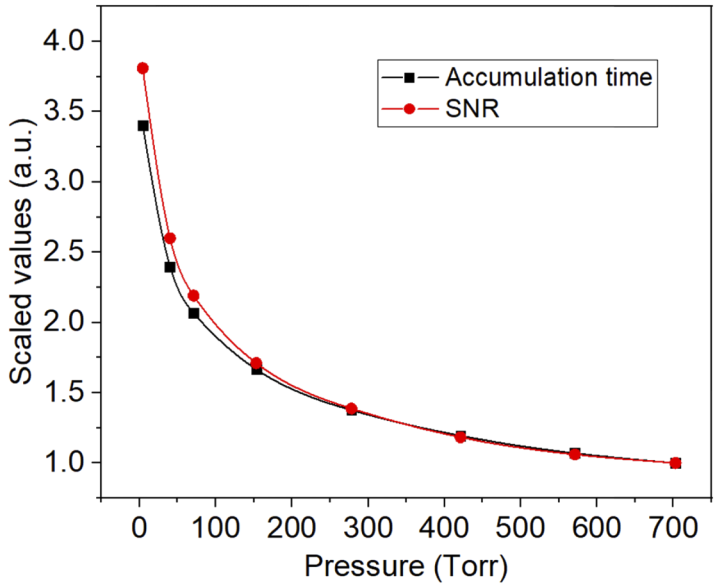

Fig. 9. Scaled values of the LITES SNR (red dots) and accumulation time (black squares). Continuous lines are guide for eye.

Optics EXPRESS

consequently of the accumulation time (see Eq. (1)). Thereby, an enhancement of the LITES signal is expected. By reducing the pressure from 700 to 5 Torr, the LITES signal, its 1σ-noise level as well as the QTF accumulation time have been measured as a function of the pressure. Since the 1σ-noise level slightly increases as the pressure decreases (when the pressure is reduced from 760 Torr to 5 Torr, the noise level increases only of 10%), the SNR has been selected as figure of merit to describe the QTF performance when used as an optical detector. For an easy comparison, both trends have been reported in the same graph where QTF accumulation time and LITES SNR have been normalized to the values obtained at atmospheric pressure. The results are shown in Fig. 9.

As the pressure increases, the LITES SNR follows almost the same trend as the QTF accumulation time, confirming the above assumptions. At 5 Torr, LITES SNR results ~13500, i.e. ~4 times higher than that obtained at atmospheric pressure, and ~6.5 times higher than that measured by using the commercial photodetector. Following the trend reported in Fig. 9 at pressures lower than 5 Torr, an increase of the LITES signal is expected because the QTF quality factor further increases. However, high quality factors determine narrow detection bandwidths that can negatively affect the frequency stabilization in a wavelength modulation TDLAS configuration. Moreover, as the quality factor increases, the QTF thermal noise increases as well. Both phenomena would prefigure an increase of the 1σ-noise level when the pressure is too low, thus deteriorating the overall LITES SNR.

4. Conclusion

In this work, QTFs were employed as photodetectors in a TDLAS sensor, exploiting the light-induced thermo-elastic effect occurring when the laser light hits a QTF surface. A set of six different QTFs was employed to study in detail the dependence of the LITES signal from the resonance properties of the resonators. The 3D strain field distributions while prongs vibrate at the fundamental and the first overtone flexural eigenmodes were modelled by using COMSOL MultiPhysics. When the laser beam was focused on the quartz surface where the maximum strain field occurs, the LITES signal-to-noise ratio is proportional to the product of the strain and the QTF accumulation time. By reducing the pressure of air surrounding the QTF from 700 Torr to 5 Torr, an increase of the SNR of a factor of ~4 has been obtained because of the corresponding increase of the QTF quality factor. In the best experimental conditions, QTF as light detector showed an SNR ∽6.5 times higher than that obtained by using a commercial amplified near-IR photodetector.

Funding

H2020 Marie Skłodowska-Curie Actions (project OPTAPHI, grant No. 860808); National Natural Science Foundation of China (61575113, 61622503, 61805132); Innovative Talents of Higher Education Institutions of Shanxi; THORLABS GmbH (Polysense Lab).

Acknowledgments

The authors from Dipartimento Interateneo di Fisica di Bari acknowledge the financial support from the European Union's Horizon 2020 research and innovation programme under the Marie Skłodowska-Curie project OPTAPHI, grant No. 860808 and from THORLABS GmbH within the joint-research laboratory PolySense. Lei Dong acknowledge financial support by the National Natural Science Foundation of China (Grant Nos. 61622503, 61575113 and 61805132) and program for the Innovative Talents of Higher Education Institutions of Shanxi.

Disclosures

The authors declare no conflicts of interest.

Optics EXPRESS

References

1. Y. Zaatara, J. Becharaa, A. Khourya, D. Zaouka, and J. P. Charles, "Diode laser sensor for process control and environmental monitoring," Appl. Energy **65**(1-4), 107–113 (2000).
2. L. Dong, F. K. Tittel, C. Li, N. P. Sanchez, H. Wu, C. Zheng, Y. Yu, A. Sampaolo, and R. J. Griffin, "Compact TDLAS based sensor design using interband cascade lasers for mid-IR trace gas sensing," Opt. Express **24**(6), A528–535 (2016).
3. R. Cui, L. Dong, H. Wu, S. Li, L. Zhang, W. Ma, W. Yin, L. Xiao, S. Jia, and F. K. Tittel, "Highly sensitive and selective CO sensor using a 2.33 μm diode laser and wavelength modulation spectroscopy," Opt. Express **26**(19), 24318 (2018).
4. R. Ghorbani and F. M. Schmidt, "ICL-based TDLAS sensor for real-time breath gas analysis of carbon monoxide isotopes," Opt. Express **25**(11), 12743–12752 (2017).
5. B. Lins, P. Zinn, R. Engelbrecht, and B. Schmauss, "Simulation-based comparison of noise effects in wavelength modulation spectroscopy and direct absorption TDLAS," Appl. Phys. B **100**(2), 367–376 (2010).
6. R. Lewicki, M. Jahjah, Y. Ma, P. Stefanski, J. Tarka, M. Razeghi, and F. K. Tittel, "Current status of mid-infrared semiconductor laser based sensor technologies for trace gas sensing applications. The Wonder of Nanotechnology: Present and Future of Optoelectronics Quantum Devices and Their Applications", 597–632 (2013).
7. J. Haas and B. Mizaikoff, "Advances in mid-infrared spectroscopy for chemical analysis," Annu. Rev. Anal. Chem. **9**(1), 45–68 (2016).
8. P. Werle, F. Slemr, M. Gehrtz, and C. Bräuchle, "Wideband noise characteristics of a lead-salt diode laser: possibility of quantum noise limited TDLAS performance," Appl. Opt. **28**(9), 1638–1642 (1989).
9. U. Willer, A. Pohlkütter, W. Schade, J. Xu, T. Losco, R. P. Green, A. Tredicucci, H. E. Beere, and D. A. Ritchie, "Resonant tuning fork detector for THz radiation," Opt. Express **17**(16), 14069–14074 (2009).
10. N. Liu, S. Zhou, L. Zhang, B. Yu, H. Fischer, W. Ren, and J. Li, "Standoff detection of VOCs using external cavity quantum cascade laser spectroscopy," Laser Phys. Lett. **15**(8), 085701 (2018).
11. Y. He, Y. Ma, Y. Tong, X. Yu, and F. K. Tittel, "Ultra-high sensitive light-induced thermoelastic spectroscopy sensor with a high Q-factor quartz tuning fork and a multipass cell," Opt. Lett. **44**(8), 1904–1907 (2019).
12. Y. Ma, Y. He, Y. Tong, X. Yu, and F. K. Tittel, "Quartz-tuning-fork enhanced photothermal spectroscopy for ultra-high sensitive trace gas detection," Opt. Express **26**(24), 32103–32110 (2018).
13. Q. Zhang, J. Chang, Z. Cong, and Z. Wang, "Application of Quartz Tuning Fork in Photodetector Based on Photothermal Effect," IEEE Photonics Technol. Lett. **31**(19), 1592–1595 (2019).
14. Y. Ma, Y. He, P. Patimisco, A. Sampaolo, S. Qiao, X. Yu, F. K. Tittel, and V. Spagnolo, "Ultra-high sensitive trace gas detection based on light-induced thermoelastic spectroscopy and a custom quartz tuning fork," Appl. Phys. Lett. **116**(1), 011103 (2020).
15. L. Hu, C. Zheng, Y. Zhang, J. Zheng, Y. Wang, and F. K. Tittel, "Compact all-fiber light-induced thermoelastic spectroscopy for gas sensing," Opt. Lett. **45**(7), 1894 (2020).
16. Hitran Database. Available online: https://hitran.org/ (accessed on 1 November 2019).
17. P. Patimisco, A. Sampaolo, L. Dong, M. Giglio, G. Scamarcio, F. K. Tittel, and V. Spagnolo, "Analysis of the electro-elastic properties of custom quartz tuning forks for optoacoustic gas sensing," Sens. Actuators, B **227**, 539–546 (2016).
18. P. Patimisco, A. Sampaolo, L. Dong, F. K. Tittel, and V. Spagnolo, "Recent advances in quartz enhanced photoacoustic sensing," Appl. Phys. Rev. **5**(1), 011106 (2018).
19. P. Patimisco, A. Sampaolo, H. Zheng, L. Dong, F. K. Tittel, and V. Spagnolo, "Quartz–enhanced photoacoustic spectrophones exploiting custom tuning forks: a review," Adv. Phys.: X **2**(1), 169–187 (2017).
20. L. Dong, A. Kosterev, D. Thomazy, and F. K. Tittel, "QEPAS spectrophones: design, optimization and performance," Appl. Phys. B **100**(3), 627–635 (2010).
21. M. Giglio, G. Menduni, P. Patimisco, A. Sampaolo, A. Elefante, V. M. N. Passaro, and V. Spagnolo, "Damping Mechanisms of Piezoelectric Quartz Tuning Forks Employed in Photoacoustic Spectroscopy for Trace Gas Sensing," Phys. Status Solidi A **216**(3), 1800552 (2019).
22. S. Li, H. Wu, R. Cui, A. Sampaolo, P. Patimisco, V. Spagnolo, F. K. Tittel, and L. Dong, "Piezo-enhanced acoustic detection module for mid-infrared trace gas sensing using a grooved quartz tuning fork," Opt. Express **27**(24), 35267–35278 (2019).
23. S. Li, L. Dong, H. Wu, A. Sampaolo, P. Patimisco, V. Spagnolo, and F. K. Tittel, "Ppb-level quartz-enhanced photoacoustic detection of carbon monoxide exploiting a surface grooved tuning fork," Anal. Chem. **91**(9), 5834–5840 (2019).
24. P. Patimisco, A. Sampaolo, M. Giglio, S. Dello Russo, V. Mackowiak, H. Rossmadl, A. Cable, F. K. Tittel, and V. Spagnolo, "Tuning forks with optimized geometries for quartz-enhanced photoacoustic spectroscopy," Opt. Express **27**(2), 1401–1415 (2019).
25. https://www.thorlabs.com/thorproduct.cfm?partnumber=PDA10CF-EC